Helical BN and ZnO nanotubes with intrinsic twisting: An objective molecular dynamics study

D.-B. Zhang,[1] E. Akatyeva,[1] and T. Dumitrică[1,2,*]

[1]*Department of Mechanical Engineering, University of Minnesota, Minneapolis, MN 55455, USA*

[2]*Department of Materials Science, University of Minnesota, Minneapolis, MN 55455, USA*

(Received 7 June 2011; published 21 September 2011)

We investigate helical single-walled nanotubes of BN and ZnO described with density-functional based tight-binding models. The employed objective molecular dynamics computational framework accounts for the helical instead of the translational symmetry and allows for simulating chiral nanotubes as the result of the nanomechanical process of a nearly axial glide [D.-B. Zhang, R. D. James, and T. Dumitrică, J. Chem. Phys. **130**, 071101 (2009)]. At large diameters, by comparing the microscopic strain stored in the tube wall with the continuum predictions, we observe the invalidity of the continuum shell idealization of the one-atom thick layer. At small diameters, comparing the computed Eshelby twist executed by the one-atom thick layers with the one predicted by pure rolling, we find that a large catalog of nanotubes store intrinsic twists. This unusual intrinsic twist effect is shown to be dependent on chirality and diameter, as part of the general trend to depart from the standard rolled-up construction. While changes in the electronic structures and Young's modulus are dominated by curvature, the shear elastic constants vary both with curvature and chirality.

DOI: 10.1103/PhysRevB.84.115431 PACS number(s): 62.23.Kn, 62.25.−g, 62.20.D−

I. INTRODUCTION

Nanostructured tubular materials have attracted vast attention for almost two decades. In addition to carbon nanotubes (CNTs), first reported in 1991,[1] a large number of inorganic nanotube (NT) nanostructures have been synthesized from both layered[2–10] and nonlayered materials.[11–16] While the inorganic fullerene-like NTs can be typically imagined as layers rolled into cylindrical structures, the NTs made out of nonlayered materials are essentially pristine one-dimensional (1D) monocrystalline structures possessing a central vacant space. In this paper, we focus on two such one-atom thick NTs made out of BN and ZnO.

Recent experimentation[14–18] indicates that screw-dislocation growth represents a growth mechanism of quasi-1D structures. Such developments renewed the interest in chiral structures other than CNTs. Due to the inherent difficulties encountered at the nanoscale, experimental characterization of these chiral materials is often problematic. Although microscopic simulations are essential tools for investigating infinite crystalline systems, their applicability in NT chiral structures is challenging due to the difficulties associated with handling translational symmetry. It is known that a screw dislocation lying parallel with the axis of a thin rod or a tube, see Fig. 1, is stabilized at a central location by an Eshelby twist.[19,20] According to the elasticity theory, the twist per unit length (a twist rate) γ'_E induced by the presence of an axial screw dislocation in an isotropic thin cylindrical rod or a tube can be expressed in terms of its outer and inner radii (R and r, respectively) and the magnitude of the Burgers vector b as

$$\gamma'_E = \frac{b}{\pi(R^2 + r^2)}. \tag{1}$$

The formation energy per unit length of a screw-dislocated isotropic thin rod or a tube writes

$$E = \frac{Gb^2}{4\pi} \ln \frac{R}{r} - \frac{Gb^2}{4\pi} \frac{R^2 - r^2}{R^2 + r^2} + S, \tag{2}$$

where G is the shear modulus. The above expression contains three different terms: the energy associated with the elastic strain field created by the screw dislocation (first term), the energy reduction attributed to the Eshelby twist (second term), and the surface energy (third term) of both outer and inner surfaces for nonlayered materials (ZnO) or bending energy related with the rolling of a sheet into a tube for layered materials (C, BN).

From a continuum perspective, the one-atom-thick tube can be represented by a shell of a certain thickness, i.e., $r \neq R$. Then, the first two terms in Eq. (2) bring nonvanishing contributions and the NT total strain energy will contain shear strain. Alternatively, the monolayer can be represented by a continuum membrane without thickness,[21] i.e., $r = R$. Then, the first two terms in Eq. (2) vanish. This implies that there is no shear energy cost to create an axial screw dislocation and, hence, the Burgers vector magnitude can be large.

Because, in general, the mechanics of an axial glide in a nanostructure is not yet understood, the magnitude of the atomic-scale Eshelby twist, and hence the resulting translational periodicity, is not *a priori* known. This makes it difficult to carry out systematic microscopic calculations in the standard periodic framework.

Efficient microscopic modeling of screw-dislocated NTs was only recently performed[22] due to the development of objective molecular dynamics (MD),[23] a relatively new microscopic technique based on the objective structures[24] concept. By coupling[25] it with the computationally efficient density-functional-based tight-binding (DFTB) treatment of the chemical binding implemented in the code TROCADERO,[26] objective MD enables simulating with minimal symmetry constraints the interplay between the classical ionic and quantum electronic degrees of freedom under an arbitrary twist and chirality.

Using objective MD and well-tested two-center nonorthogonal DFTB models,[27–29] in this paper, we investigate the nanomechanics of screw dislocations in one-atom-thick hexagonal layers of BN and ZnO. The motivation for our study is threefold.

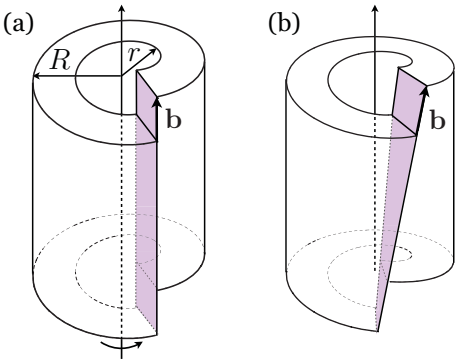

FIG. 1. (Color online) Schematics of a screw-dislocated hollow tube with Burgers vector b with (a) fixed ends and (b) one free-to-rotate end leading to an Eshelby's twist.

Firstly, it is interesting to understand and compare the rolling traits of these two materials as they are representative for the two categories of the currently synthesized helical NTs. Bulk hexagonal BN is a layered material and BN NTs have been synthesized in both single- and multiwalled forms.[4–7,9] Although the majority of obtained tubes displayed zigzag configurations, helical and armchair BN NTs were also reported. ZnO exhibits a typical wurtzite structure and helical ZnO NTs have been synthesized along the c direction via dislocation-driven growth.[14–16] Structurally, the thicker-walled ZnO NTs are faceted and display a hexagonal cross section.[12,14–16] The single-walled NTs have a ZnO hexagonal wall and a cylindrical cross section.[30]

Secondly, single-walled BN and ZnO NTs are analogous to CNTs, with alternating B (Zn) and N (O) atoms substituting for C atoms. They are both isotropic in the linear elastic regime. When this approximation holds, the magnitude of the Eshelby twist can be analytically predicted based on the standard rolled-up construction of CNTs.[31] Recent investigations[32,33] indicated that the thicker, three atomic layers of MoS_2 and TiS_2 exhibit a departure from the rolled-up predictions, manifested in diameter-, chirality-, and wall-structure-dependent intrinsic twists. Other symmetry-constrained DFTB calculations[34] indicated that even the widely studied CNTs exhibit intrinsic twist. The effect was attributed[34] to the well-known strain sensitivity of the electronic properties.[37] It would be interesting to know if such intrinsic twists are present in other one-atom-thick NTs with electronic properties less sensitive to twisting.

Thirdly, the BN NTs offer a number of appealing properties,[9,39–41] including excellent mechanical properties.[38,42] They are interesting as components for electromechanical devices in which the individual BN NT is subjected to torsional deformation.[43] The knowledge of the elastic constant variations with diameter and chirality is assistive for the design of such nanodevices.

This paper is organized as follows. Section II A reviews the standard rolled-up construction and details the original helical nanotube construction introduced by Iijima[1] and employed in Ref. 32 and 33 to simulate chiral MoS_2 and TiS_2 nanotubes. The relation between the Eshelby twist and the helical NT indexes n and m is indicated. Section II B outlines the helical symmetry treatment of the electronic states. Section III presents the simulation results for both BN and ZnO helical NTs. Section III A focuses on the obtained structures and compares them with the ideal rolled-up structure predictions. For a comparison with the existing literature,[34,44] the case of small-diameter helical CNT structures is also considered. Section III B focuses on the scaling of electromechanical properties with chirality and diameter. Finally, in Sec. IV obtained results are summarized and discussed.

II. METHODOLOGY

A. Ideal nanotube structure

An (n,m) NT is commonly conceptualized in the literature by the rolled-up construction, which involves pure mechanical rolling of a flat hexagonal-lattice strip along the (n,m) hexagonal lattice vector into a seamless cylinder.[31] In the unrolled representation, the n and m indices represent the components of the chiral vector $\mathbf{C_h}$ of the nanotube on the lattice vectors $\mathbf{a_1}$ and $\mathbf{a_2}$ of the honeycomb lattice, i.e., $\mathbf{C_h} = n\mathbf{a_1} + m\mathbf{a_2}$. By convention, $\mathbf{a_1}$ and $\mathbf{a_2}$ are taken along the two zigzag chains as shown in Fig. 2. The radius of this tubule writes $R_0 = |\mathbf{C_h}|/2\pi = a\sqrt{n^2 + nm + m^2}/2\pi$. Here, a is the length of the primitive vector of the flat layer. The NT chirality is measured by the angle $\chi = \arcsin[(\sqrt{3}m)/(2\sqrt{n^2 + nm + m^2})]$

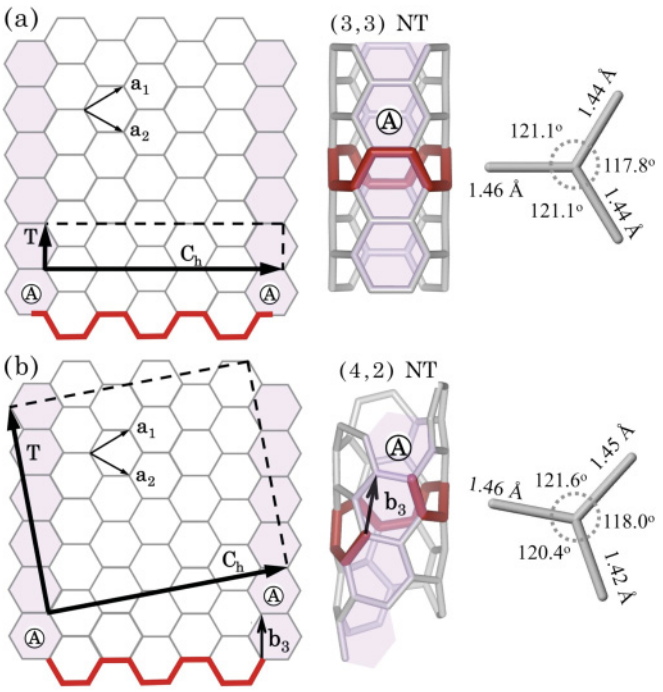

FIG. 2. (Color online) (left and center) Schematics for the two ways of forming (a) (3,3) and (b) (4,2) NTs from the ideal flat hexagonal layer: by rolling-up the big rectangle bounded by the chiral $\mathbf{C_h}$ and translational $\mathbf{T}$ vectors and by rolling-up a ribbon such as the hexagons labeled by A become superimposed. Lattice basis vectors $\mathbf{a_1}$, $\mathbf{a_2}$, and Burgers vector $\mathbf{b_3}$ along the hatched hexagon are also shown. The row of hatched hexagons form a helix on the tube. The objective unit cells used in the calculations are shown with thicker (red) lines. (right) Bond lengths and angles obtained by mapping in two dimensions the DFTB optimized CNTs. The NT axis is in the vertical direction.

enclosed by $\mathbf{C_h}$ and the closest of the three zigzag chains in the flat graphene sheet. The special cases corresponding to $(n,0)$ and (n,n) are the zigzag and armchair configurations, respectively.

The fundamental property of an infinitely long NT is ostensibly its translational periodicity, described by the translational vector $\mathbf{T}$ pointing along the axial direction of the NT. In the unrolled representation, the translational vector $\mathbf{T}$ is orthogonal to $\mathbf{C_h}$. While the precise expression of $\mathbf{T}$ can be found in literature,[31] what matters here is that it points into a direction, which is distinct from one of the glide directions of the graphene sheet, see Fig. 2. The underlying assumption is that during the rolling process of the unit cell delineated by $\mathbf{T}$ and $\mathbf{C_h}$, the translational symmetry is preserved even though the bond lengths and angles between atoms will change due to finite curvature effects. The infinitely long NT structure is then described with

$$\mathbf{X}_{j,\zeta} = \mathbf{X}_j + \zeta\mathbf{T}, \tag{3}$$

where $\mathbf{X}_j$ are the coordinates of the atoms located in the unit cell. Integer ζ indexes the unit cell replica.

An ideal NT possesses also helical symmetry, described in the unrolled representation by screw vectors comprised of both rotational and translational components, i.e., with components along both $\mathbf{C_h}$ and $\mathbf{T}$. One such vector is the Burgers vector $\mathbf{b_3} = \mathbf{a_1} - \mathbf{a_2}$, shown in Fig. 2. By evaluating its axial and circumferential components, one obtains that screw vector $\mathbf{b_3}$ is associated with a θ_0 angular rotation and a T_0 axial translation given by

$$\begin{aligned} \theta_0 &= \frac{\pi(n-m)}{n^2+nm+m^2}, \\ T_0 &= \frac{\sqrt{3}a(n+m)}{2\sqrt{n^2+nm+m^2}}. \end{aligned} \tag{4}$$

The makeup of helical CNTs was depicted by Iijima in a another way, namely, by the rolling-up along the tube axis of a graphene ribbon in the armchair orientation (along the glide direction indicated by the Burgers vector $\mathbf{b}_3$), see Fig. 2, such that the hatched edge hexagons are superimposed.[1] In the cylindrical geometry, the gliding of the edges past one another creates an axial screw dislocation. Indeed, in the cylindrical structure of an (n,n) NT, its chiral vector keeps a closed ring composed of $4n$ atoms. A slip along the nearly axial helical glide path introduces an integer number of hexagons i between the head and the tail of the old chiral vector and thus leads to a change in NT's chirality. Of course, during this process the cylindrical structure of the armchair NT is maintained and its new chiral vector keeps a closed ring, i.e., the dislocation between the head and the tail of the new chiral vector is zero. The wrapping indexes of the new chiral pattern can be easily obtained by identifying on the unrolled NT representation the new chirality vector connecting the overlapping hexagons. It is an easy task to show that one glide step introduces a characteristic $(+1,-1)$ change in NT's indexes.[22] The repeated glide defines a nearly equal radius family of NTs with indexes $(n,n),(n+1,n-1),\ldots,(2n,0)$. An arbitrary NT with indexes $(n+i,n-i)$, where $i \in [0,n]$, can be viewed as a screw-dislocated (n,n) NT that underwent a twist per unit length given by

$$\gamma_0 = \frac{\theta_0}{T_0} = \frac{b}{2\pi R_0^2\sqrt{1-\left(\frac{b}{2\pi R_0}\right)^2}}. \tag{5}$$

Here, $b = i|\mathbf{b_3}|$ is the magnitude of the Burgers vector. According to Eq. (1), the twist rate for an one-atom-thick tube, where inner and outer radii coincide, is $\gamma'_E = b/2\pi R_0^2$. This means that the twist rate calculated under pure rolling assumption, as given in Eq. (5), converges to the continuum membrane elasticity result when the tube radius increases (valid for $i < n$). Even for the extreme case of zigzag NT $(i = n)$, the calculated twist rate of $\gamma_0 = b/\sqrt{3}\pi R_0^2$ is very close to continuum predictions.

What is useful in the screw-dislocation construction based on the nearly-axial glide is that under the helical repetition rule indicated by $\mathbf{b_3}$, one can alternatively describe any NT from this family based on the same $4n$ atoms contained in the small translational unit cell of the armchair (n,n) NT. Let $\mathbf{X}_j$ be the atomic positions in the open ring after the axial glide took place. Positions $\mathbf{X}_{j,\zeta}$ of the atoms located in the objective cell replica indexed by integer ζ are then obtained with

$$\mathbf{X}_{j,\zeta} = \mathbf{Q}^\zeta\mathbf{X}_j + \zeta\mathbf{T_0},\ j = 1,\ldots,4n. \tag{6}$$

The rotational matrix $\mathbf{Q}$ and the axial vector $\mathbf{T_0}$

$$\mathbf{Q} = \begin{pmatrix} \cos\theta_0 & -\sin\theta_0 & 0 \\ \sin\theta_0 & \cos\theta_0 & 0 \\ 0 & 0 & 1 \end{pmatrix}, \quad \mathbf{T_0} = \begin{pmatrix} 0 \\ 0 \\ T_0 \end{pmatrix}, \tag{7}$$

describe the helical transformation indicated by the screw vector $\mathbf{b}_3$.

We emphasize that other views of chiral NTs as screw-dislocated achiral NTs are possible. To address CNT growth,[36] an ingenious representation was proposed that involves $(n,0)$, $(n,1),\ldots,(n,n)$ NTs obtained via glides along $-0.5\mathbf{a}_1 + \mathbf{a}_2$ combined with addition and removal of atom chains. The representation used here based on Iijima's construction of helical NTs, has relevance in the torsional mechanical response.[22] It connects (n,n), $(n+1,n-1),\ldots,(2n,0)$ NTs without involving any edge component.

B. Symmetry-adapted tight-binding objective molecular dynamics

With the NT description (3), the usual DFTB treatment formulated under periodic boundary conditions can be applied in order to determine the precise atomic location inside one unit cell.[26] Microscopic modeling based on description (6), however, requires special consideration for the electronic states. The one-electron states are represented in terms of symmetry-adapted Bloch sums

$$|\alpha j,\kappa\rangle = \frac{1}{\sqrt{N_s}}\sum_{\zeta=0}^{N_s-1} e^{i\kappa\zeta}|\alpha j,\zeta\rangle, \tag{8}$$

where N_s is the number of helical operations (typically ∞) over which the cyclic boundary conditions are imposed. The Bloch factors are eigenvalues of the helical operators and $-\pi \leqslant \kappa < \pi$ is the helical quantum number. $|\alpha j\rangle$ is an atomic orbital with symmetry α located on atom j inside

the computational cell. The valence shell basis set used here comprises sp basis functions for C, B, N, and O and sd for Zn. The orbitals located in the objective cell indexed by ζ are obtained by applying proper rotations to the corresponding $|\alpha j\rangle$ orbitals.[25] Specifically, for the five d orbitals of Zn, we have

$$\begin{bmatrix} |d_{x^2-y^2}j,\zeta\rangle \\ |d_{xy}j,\zeta\rangle \\ |d_{zx}j,\zeta\rangle \\ |d_{yz}j,\zeta\rangle \\ |d_{3z^2-r^2}j,\zeta\rangle \end{bmatrix} = \begin{bmatrix} \cos 2\theta & -\sin 2\theta & 0 & 0 & 0 \\ \sin 2\theta & \cos 2\theta & 0 & 0 & 0 \\ 0 & 0 & \cos\theta & -\sin\theta & 0 \\ 0 & 0 & \sin\theta & \cos\theta & 0 \\ 0 & 0 & 0 & 0 & 1 \end{bmatrix} \begin{bmatrix} |d_{x^2-y^2}j\rangle \\ |d_{xy}j\rangle \\ |d_{zx}j\rangle \\ |d_{yz}j\rangle \\ |d_{3z^2-r^2}j\rangle \end{bmatrix}, \tag{9}$$

where $\theta = \zeta\theta_0$. Note that the $d_{3z^2-r^2}$ orbitals are invariant because they are oriented along z axis, which is parallel to the NT axis.

The symmetry-adapted Bloch elements with different helical numbers of the TB Hamiltonian and overlap matrices vanish. Therefore, the eigenvalue problem becomes block diagonal and it can be solved separately for each block labeled by κ. As described elsewhere,[25] the total energy and the forces on each atom are then computed analytically using the Hellmann-Feynman theorem.

III. RESULTS

Using the DFTB symmetry-adapted theoretical framework, we have performed objective calculations on four NT families ($n = 3,6,8,10$) generated by introducing axial screw dislocations in (n,n) NT structures. Additionally, a large collection of armchair and zigzag NTs in the 1–4 nm diameter range was considered. For a comparison, the systematic calculations performed on BN and ZnO NTs, were supplemented with calculations carried out on selected small-diameter CNTs.

The linear combinations of atomic orbitals were sampled for 50 κ values of the helical Bloch phase. The initial structural information for any NT is adopted from the rolled-up approximation, for which the free parameters θ_0 and T_0 can be obtained with the simple expressions given before. Next, the stress-free atomic positions and the actual DFTB Eshelby's twist parameters θ_E and T_E are identified by applying a conjugate gradient minimization procedure to the potential energy.

A. Optimized nanotube structures

One advantage of the current approach is that it enables us to separate the curvature from the chirality effects. The first goal is to determine how well the translational symmetry and the ideal rolled-up predictions hold. The results of our structural optimizations indicate that only for small-diameter chiral NTs, the axial relaxation under fixed angle θ_0 is not sufficient to obtain the stress-free states. As exemplified in Fig. 3, for the (3,3)...(6,0) NT family, further angular relaxation under fixed T_E exhibits a parabolic dependence and can lower the energy. The angle values of the stress-free chiral structures θ_E deviate from the predicted θ_0.

Unlike the flat layer, the structure of these narrow NTs is characterized by nonequal bond lengths and bond angles. The data for (4,2) NTs summarized in Table I, detail the significant departure from the bond lengths and angles given by the rolled-up prediction. The most circumferentially oriented bonds are the most affected. For example, while the rolled-up prediction gives a 1.399 Å length for the most circumferential bonds in a (4,2) CNT, the DFTB relaxations obtained a 1.430 Å value. Such microscopic relaxations lead to differences not only between the optimized R and nonoptimized R_0 radii, but also between the optimized θ_E and T_E and the nonoptimized θ_0 and T_0 structural parameters. Hence, with respect to the the rolled-up construction, the (4,2) NT structures store both circumferential and helical prestrains.

The presence of helical prestrains alters the translational unit cells identified on the ideal flat hexagonal layer. To illustrate this point, we mapped in two dimensions the DFTB

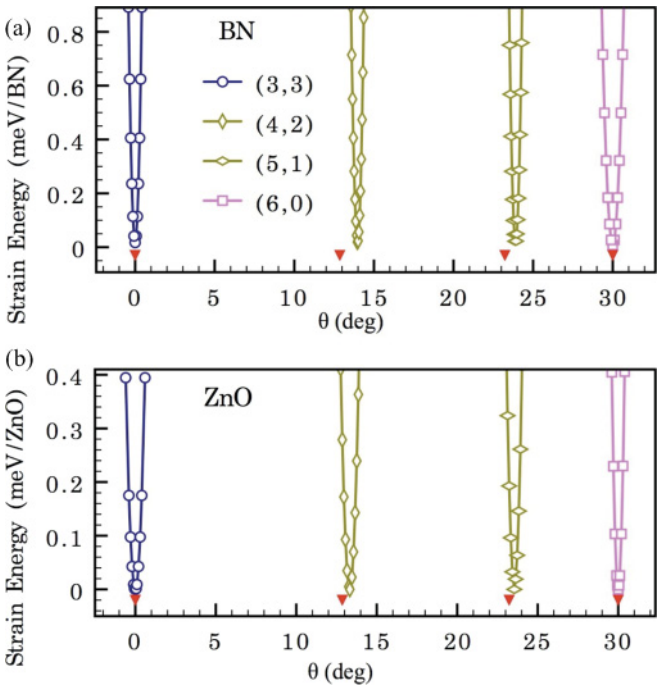

FIG. 3. (Color online) Torsional strain energy vs θ for the (3,3), (4,2), (5,1), and (6,0) (a) BN and (b) ZnO NTs. The energy minima indicate the θ_E angles of the stress-free NTs, while the arrowheads indicate the θ_0 values.

TABLE I. The DFTB structure of (4,2) BN, ZnO, and C NTs compared with the rolled-up predictions.

Material:	BN	ZnO	C
Bond lengths (Å):			
DFTB	1.476, 1.463, 1.495	1.925, 1.913, 1.922	1.430, 1.420, 1.449
Rolled-up predictions	1.424, 1.450, 1.445	1.870, 1.904, 1.898	1.399, 1.425, 1.420
DFTB mapped in 2D	. . .	. . .	1.456, 1.420, 1.454
Bond angles (deg):			
DFTB	119.6, 117.0, 119.5	119.5, 119.2, 117.8	118.4, 119.1, 115.1
Rolled-up predictions	118.1, 120.3, 113.2	118.1, 120.3, 113.2	118.1, 120.3, 113.2
DFTB mapped in 2D	. . .	. . .	120.4, 118.0, 121.6
NT Radius (Å):			
DFTB	2.210	2.852	2.142
Rolled-up predictions	2.115	2.778	2.079
Structural parameters:			
DFTB T_E (Å), θ_E (deg)	2.470, 13.96	3.240, 13.33	2.411, 13.42
Rolled-up T_0(Å),θ_0 (deg)	2.466, 12.86	3.239, 12.86	2.424, 12.86
Buckling (Å)			
DFTB	0.125	0.134	0
Rolled-up predictions	0	0	0

relaxed structures of the (3,3) and (4,2) CNTs. The obtained bond lengths and angles, depicted in Fig. 2 (right), reflect into a deformed hexagonal layer. For the (3,3) CNT, the lattice is elongated along the $\mathbf{C_h}$ and $\mathbf{T}$ directions, which remain perpendicular onto each other. However, for the (4,2) CNT case the lattice is additionally sheared and vector $\mathbf{T}$ acquires a small component along $\mathbf{C_h}$, thus becoming a screw vector. Hence, the translational symmetry depicted by the translation vector $\mathbf{T}$ is broken by the intrinsic twist $(\theta_E - \theta_0)/T_E$.

Our calculations indicated that both BN and ZnO NTs store intrinsic twists. Focusing on the (3,3) . . . (6,0) NT family, Table II reveals that at a set chirality, BN NTs exhibit the largest intrinsic twist. For the CNT family, we are able to regain the intrinsic twist values reported earlier[34] from calculations based on higher symmetry two-atoms "helical-angular" cells.

To give a broader view of the deviations from the ideal rolled-up construction, Figs. 4 and 5 plot the variations with the NT diameter of the axial prestrain $\varepsilon = (T_E - T_0)/T_0$, the radial prestrain, defined as $\varepsilon^* = (R - R_0)/R_0$, the buckling of the surface, defined as the mean radius of the N (O) atoms minus the mean radius of the B (Zn) atoms, and the shear prestrain, defined as $\gamma = R(\theta_E - \theta_0)/T_E$. The obtained changes in NT length and diameter, buckling of the surface, and locking of the intrinsic twist are qualitatively similar for BN and ZnO. We obtain the following insights: (i) the rolled-up construction works very well for both BN and ZnO only at diameters larger than ∼2 nm. (ii) As the NT diameter decreases, ε displays an increased spread after chirality. In the nearly equal diameter families, the armchair tubes are the most elongated while the zigzag ones are the most compressed. (iii) As the NT diameter decreases, ε^* is also significant but appears to be chirality independent. Our data can be fitted with the power laws $\varepsilon^* = 2.2(R/\text{Å})^{-2.3}$ for BN and $\varepsilon^* = 0.2(R/\text{Å})^{-2}$ for ZnO. (iv) The amount of buckling is independent of the tube helicity as well. In BN and ZnO NTs, the wall bucking is however present to some degree even at large diameters, as reflected by the scaling laws $0.6(R/\text{Å})^{-1}$ Å for BN and $0.4(R/\text{Å})^{-1}$ for ZnO obtained by fitting the atomistic data presented in Figs. 4(c) and 5(c). Finally, (v) the γ stored in the NT's wall is both diameter and chirality dependent. It is significant only at the smallest diameters. As can be seen in Figs. 4(d) and 5(d), γ is absent in the armchair and zigzag NTs and it is maximal near the 15° chirality.

TABLE II. Intrinsic twist values (deg/nm) in (3,3) . . . (6,0) NT family, as obtained with the DFTB description.

Material:	BN	ZnO	C
(3,3)	0	0	0
(4,2)	4.5	1.5	2.3
(5,1)	2.8	1.0	1.1
(6,0)	0	0	0

For a compact characterization of the NT structural parameters, we appeal to simple functional forms constructed based on symmetry arguments. At constant R, the developed anisotropy between special armchair and zigzag directions implies that both the ε and γ prestrains must have a 60° period in their chirality angle dependence. Additionally, we find that the radial scaling laws identified for ε^* are suitable for ε and γ data as well. Indeed, Figs. 4(e), 4(f), 5(e), and 5(f) show nearly linear dependences of the $R^{2.3}$ and R^2 augmented ε and γ to the lowest symmetry-allowed order in chiral angle. Specifically, we obtained $\varepsilon = -0.12(R/\text{Å})^{-2.3}\cos(6\chi)$ and $\gamma = 0.24(R/\text{Å})^{-2.3}\sin(6\chi)$ for BN, $\varepsilon = -0.03(R/\text{Å})^{-2}\cos(6\chi) - 0.02(R/\text{Å})^{-2}$ and $\gamma = 0.05(R/\text{Å})^{-2}\sin(6\chi)$ for ZnO. As discussed before,[44] these prestrains alter the chiral angle values. Of course, the n and m indexes are not changed. In the above expressions, χ represents the chirality predicted by the rolled-up construction.

B. Electromechanical properties

Having identified the stress-free NT morphologies, we are now in the position to analyze their electronic states. We focus our attention on ZnO NTs, since the BN NTs

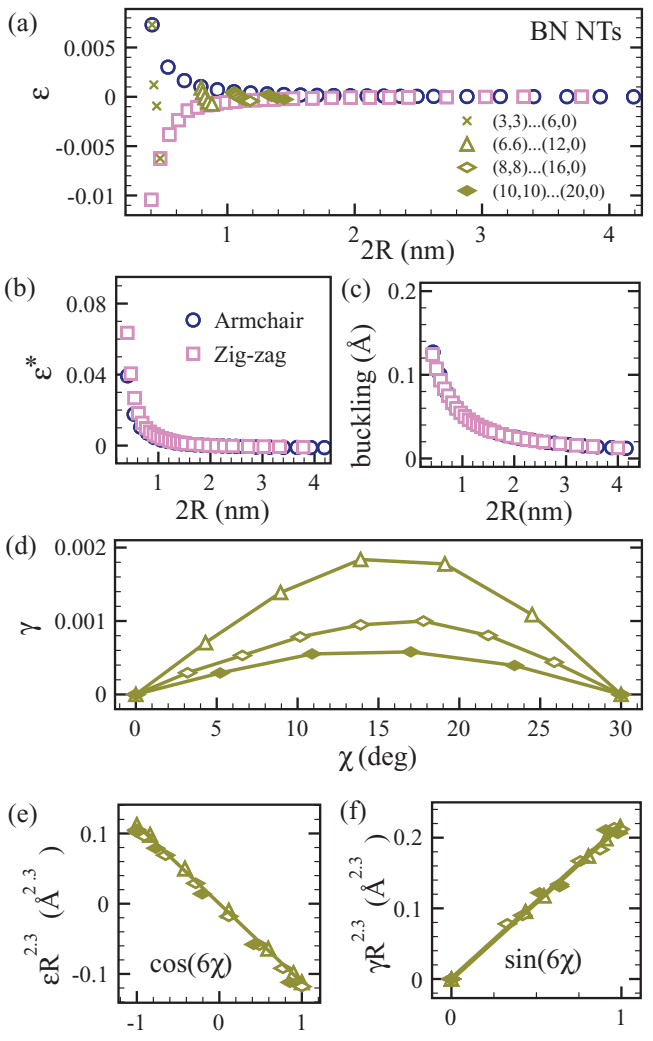

FIG. 4. (Color online) Optimized structures of BN NTs. Dependence of the intrinsic (a) axial prestrain, (b) radial prestrain, and (c) wall buckling on diameter. (d) Dependence of the intrinsic shear γ on chirality. Scaling of (e) the axial prestrain and (f) intrinsic shear prestrain (both multiplied by $R^{2.3}$) with lowest symmetry-allowed order in chiral angle.

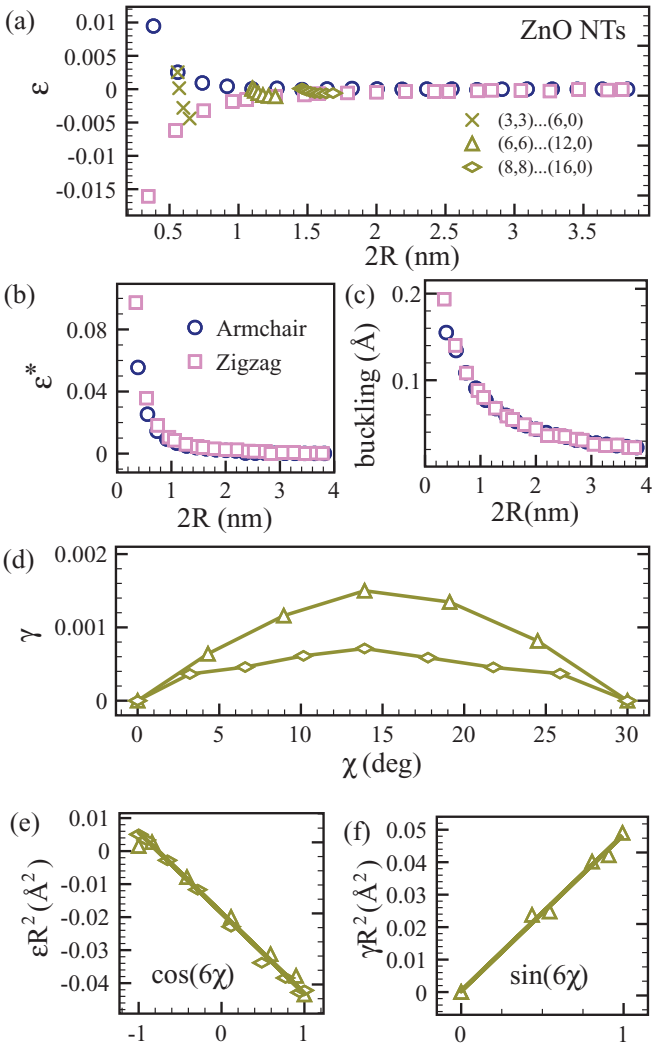

FIG. 5. (Color online) Optimized structures of ZnO NTs. Dependence of the intrinsic (a) axial prestrain, (b) radial prestrain, and (c) wall buckling on diameter. (d) Dependence of the intrinsic shear γ on chirality. Scaling of (e) the axial prestrain and (f) intrinsic shear prestrain (both multiplied by R^2) with lowest symmetry-allowed order in chiral angle.

have already been the focus of other studies.[40] The DFTB parametrization is designed to describe well the structural properties of ZnO materials. Unfortunately, it overestimates the band-gap values. For example, the used parametrization predicts a band gap of 6.3 eV for the bulk wurtzite ZnO phase, while the experimentally measured value is 3.4 eV. For the purposes of predicting the fundamental band gaps in ZnO NTs, the original parameters have been slightly altered: the on-site energy value for the 4*s* electron of Zn was replaced by the experimental first ionization energy (the parameter is changed from −0.2079 to −0.3527 a.u.). This modification ensures that the band-gap of the wurtzite phase is reproduced.[45]

Similar with BN NTs,[40] the electronic structure of ZnO NTs appears more sensitive to curvature than to chirality. The calculated band gaps of all the ZnO NTs studied are displayed in Fig. 6 as a function of their diameters. The band-gap increases with diameter. Above ∼2 nm, it converges rapidly, regardless of chirality, to the 4.08-eV value of the flat layer. Below ∼2 nm in diameter, the band gap begins to exhibit a weak dispersion after chirality, which becomes non-negligeable for the smallest-diameter NT considered here, see Fig. 6 (inset).

The electronic structures are stable against applied small twists. In objective MD, an arbitrary twist can be applied by varying θ_E while keeping T_E constant. Figure 7 exemplifies the response of the density of states (DOS) in (6,6) NTs to a 4.2 deg/nm twist rate. It can be seen that both BN and ZnO remain insensitive to small twists, especially around the Fermi level. This is in sharp contrast with the behavior of the (6,6) CNT, showing a band-gap opening and change in the location of the van Hoove singularities. This obtained behavior is in agreement with the model proposed by Yang and Han.[37]

Pure axial strain can be applied by varying T_E and keeping constant θ_E. Similarly, pure shear strain can be achieved by varying θ_E and keeping constant T_E. The adiabatic approximation, where forces on atoms are derived from the

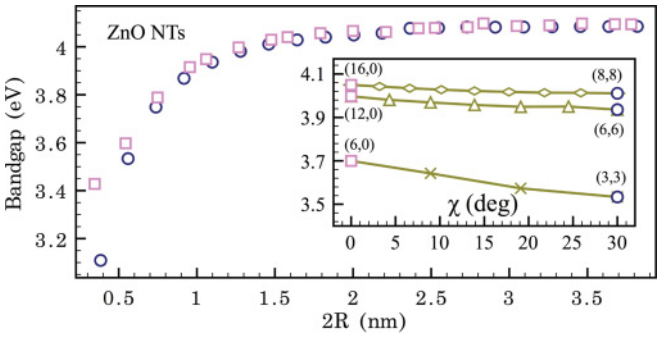

FIG. 6. (Color online) Band-gap dependence on diameter and chirality for ZnO NTs.

electronic ground state at each strain configuration, was used to study tensile and torsional deformations.[35] Our investigation was restricted to the linear elastic regime. The elastic constants were evaluated through second-order polynomial fits of the ground-state energy's dependence on strain. The obtained size dependence of Young's modulus Y is displayed in Fig. 8(a). The axial elasticity of BN NTs appears similar to the in-plane one of the flat BN sheet, apart from effects due the tube curvature. Indeed, above $\sim$2 nm in diameter, Y is practically constant and takes the 850 GPa value. For $2R <\sim 2$ nm, Y gradually softens and remains insensitive to chirality. The calculated shear modulus (G) is shown in Fig. 8(b). For $2R > \sim 2$ nm, G converges quickly to the 370 GPa value. For $2R <$ $\sim$2 nm, there is a pronounced χ splitting, with G bounded from above by zigzag and from below by armchair BN NTs.

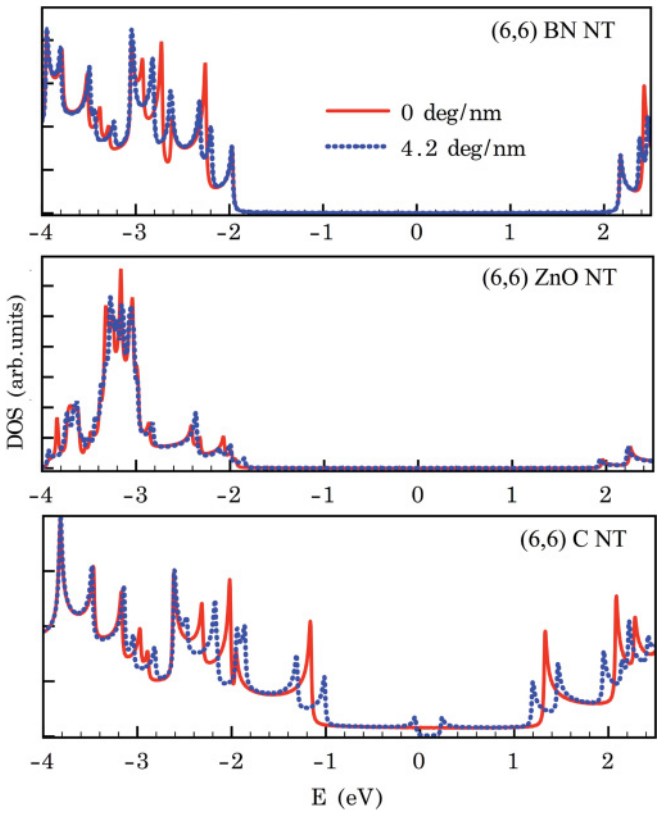

FIG. 7. (Color online) Density of states in stress-free (6,6) NTs and under 4.2 deg/nm applied twist. The Fermi energy level was set to zero.

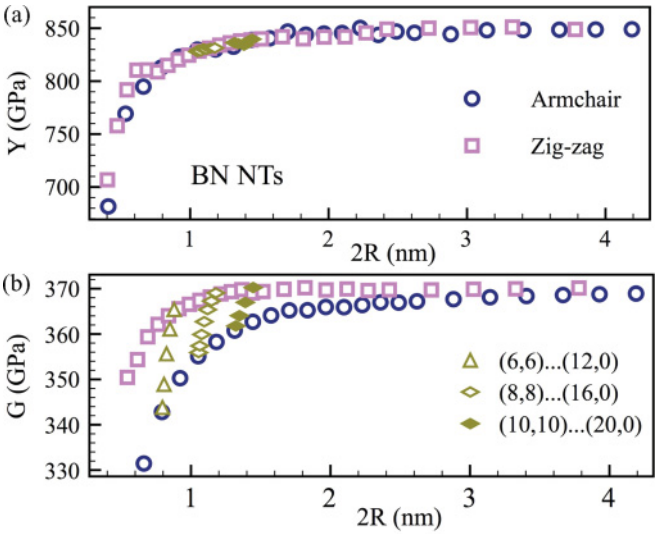

FIG. 8. (Color online) (a) Young's and (b) shear modulus vs. BN NT diameter. In order to gain GPa units, a wall thickness of 3.14 Å was assumed.

IV. DISCUSSION AND CONCLUSION

The objective molecular dynamics technique, which accounts for helical symmetry explicitly, allowed us to systematically investigate the screw dislocation mechanics in BN and ZnO monoatomic layers. We addressed a large catalog of NTs and obtained scaling laws beyond the errors of the numerical procedures.

The results shown in Figs. 4 and 5 demonstrate qualitative similarity in the rolling traits for layered BN and nonlayered ZnO materials. Differences are only qualitative in scaling laws of prestrains with the NT radius and in the magnitudes of prestrains and wall bucklings. ZnO NTs reveal smaller intrinsic twists than BN ones, but a larger buckling, as shown in Table II.

For both BN and ZnO with $2R > \sim 2$ nm, we obtained that the screw dislocation mechanics gives a structure equivalent with the rolled-up construction one. This means that, as predicted by Eq. (2) in the $r = R$ limit, chiral NTs store only small bending strain. The lack of shear strain energy in the NT wall, once more,[46] suggests the invalidity of the continuum shell idealization associated with the one-atom-thick layer. For $2R <\sim 2$ nm, the detailed structure analysis of our optimized NTs indicated a systematic departure from the rolled-up construction manifested in radial, axial, and shear prestrains that exhibit a common scaling with curvature. The presence of the shear strain, manifested in an intrinsic structural twist, removes the NT translational periodicity predicted by the rolled-up prediction. Therefore care must be exercised in future numerical studies of chiral nanotubes relying on standard translational symmetry.

The presence of the prestrains in small-diameter NTs, indicate that the NT wall stores not only bending but also in-plane axial and shear strain energy. The discrepancy with the prediction given by Eq. (2) in the $r = R$ limit is due to the loss of isotropy in the NT wall. It is useful to realize that

the axial and shear prestrains observed in smaller diameter NTs are ultimately related to the significant distortion of the hexagonal lattice symmetry.

The calculated elastic moduli of BN NTs presented in Fig. 8 reveal that Young's modulus is only curvature dependent, while shear modulus G presents both curvature and chirality dependence. The behavior at $2R <\sim 2$ nm, unequivocally shows that isotropy is lost, since the continuum isotropic relation[21] $G = Y/2(1+\nu)$ with ν the Poisson ratio cannot be used. Isotropic continuum idealization can be used for BN and ZnO NTs with $2R > \sim 2$ nm. The isotropic relation between G and Y if fulfilled with $\nu = 0.15$.

In the case of CNTs, the origin of the intrinsic twist was attributed[34] to the well-known sensitivity of the electronic states to torsion.[37] The BN and ZnO NT studied here exhibit lack of electronic-states sensitivity to chirality and twist. The common scaling of the axial, shear, and radial prestrain with curvature allows us to attribute the intrinsic twist solely to the curvature effect. The presence of prestrains in (4,2) CNT documented in Table I and in a previous work,[44] suggests that curvature plays a prime role in the development of intrinsic twist in CNTs.

ACKNOWLEDGMENT

We thank G. Seifert for providing useful comments. Computations were carried out at the Minnesota Supercomputing Institute. Work supported by NSF Grant No. DMR-1006706, NSF CAREER Grant No. CMMI-0747684, and AFOSR Grant No. FA9550-09-1-0339.

*Corresponding author: td@me.umn.edu

[1] S. Iijima, Nature (London) **354**, 56 (1991).
[2] Y. Feldman, E. Wasserman, D. J. Srolovitz, and R. Tenne, Science **267**, 222 (1995).
[3] J. Chen, S.-L. Li, Z.-L. Tao, and F. Gao, Chem. Commun. **8**, 980 (2003).
[4] N. G. Chopra, R. J. Luyken, K. Cherrey, V. H. Crespi, M. L. Cohen, S. G. Louie, and A. Zettl, Science **269**, 966 (1995).
[5] A. Loiseau, F. Willaime, N. Demoncy, G. Hug, and H. Pascard, Phys. Rev. Lett. **76**, 4737 (1996).
[6] D. Golberg, Y. Bando, M. Eremets, K. Takemura, K. Kurashima, and H. Yusa, Appl. Phys. Lett. **69**, 2045 (1996).
[7] E. Bengu and L. D. Marks, Phys. Rev. Lett. **86**, 2385 (2001).
[8] J. S. Wang, V. K. Kayastha, Y. K. Yap, Z. Y. Fan, J. G. Lu, Z. W. Pan, I. N. Ivanov, A. A. Puretzky, and D. B. Geohegan, Nano Lett. **5**, 2528 (2005).
[9] D. Golberg, Y. Bando, Y. Huang, T. Terao, M. Mitome, C. C. Tang, and C. Y. Zhi, ACS Nano **4**, 2979 (2010).
[10] L. Qin, J. Yu, M. Y. Li, F. Liu, and X. D. Bai, Nanotechnology **22**, 215602 (2011).
[11] Y. Sun, G. Fuge, N. A. Fox, D. J. Riley, and M. N. Ashfold, Adv. Mater. **17**, 2477 (2005).
[12] B. Liu and H. C. Zeng, Nano Res. **2**, 201 (2009).
[13] Y. Xi, J. H. Song, S. Xu, R. S. Yang, Z. Y. Gao, C. G. Hu, and Z. L. Wang, J. Mater. Chem. **19**, 9260 (2009).
[14] S. A. Morin, M. J. Bierman, J. Tong, and S. Jin, Science **328**, 476 (2010).
[15] S. A. Morin and S. Jin, Nano Lett. **10**, 3459 (2010).
[16] S. Jin, M. J. Bierman, and S. A. Morin, J. Phys. Chem. Lett. **1**, 1472 (2010).
[17] M. Marchand, C. Journet, D. Guillot, J.-M. Benoit, B. I. Yakobson, and S. T. Purcell, Nano Lett. **9**, 2961 (2009).
[18] M. J. Behr, K. A. Mkhoyan, and E. S. Aydil, ACS Nano **4**, 5087 (2010).
[19] J. D. Eshelby, J. Appl. Phys. **24**, 176 (1953).
[20] J. D. Eshelby, Philos. Mag. **3**, 440 (1958); K. Yoshida, Jpn. J. Appl. Phys. **10**, 565 (1964).
[21] M. Arroyo and T. Belytschko, Phys. Rev. B **69**, 115415 (2004).
[22] D.-B. Zhang, R. D. James, and T. Dumitrică, J. Chem. Phys. **130**, 071101 (2009).
[23] T. Dumitrică and R. D. James, J. Mech. Phys. Solids **55**, 2206 (2007).
[24] R. D. James, J. Mech. Phys. Solids **54**, 2354 (2006).
[25] D.-B. Zhang, M. Hua, and T. Dumitrică, J. Chem. Phys. **128**, 084104 (2008).
[26] R. Rurali and E. Hernandez, Comput. Mater. Sci. **28**, 85 (2003).
[27] D. Porezag, Th. Frauenheim, Th. Köhler, G. Seifert, and R. Kaschner, Phys. Rev. B **51**, 12947 (1995).
[28] J. Widany, Th. Frauenheim, Th. Köhler, M. Sternberg, D. Porezag, G. Jungnickel, and G. Seifert, Phys. Rev. B **53**, 4443 (1996).
[29] N. H. Moreira, A. L. da Rosa, and T. Frauenheim, Appl. Phys. Lett. **94**, 193109 (2009); C. Fisker and T. G. Pedersen, Phys. Status Solidi B **246**, 354 (2009).
[30] Z. Zhou, Y. Li, L. Liu, Y. Chen, S. B. Zhang, and Z. Chen, J. Phys. Chem. C **112**, 13926 (2008).
[31] R. Saito, G. Dresselhaus, and M. S. Dresselhaus, *Physical Properties of Carbon Nanotubes* (Imperial College Press, London, UK 1998).
[32] D.-B. Zhang, T. Dumitrică, and G. Seifert, Phys. Rev. Lett. **104**, 065502 (2010).
[33] D. Teich, T. Lorenz, J.-O. Joswig, G. Seifert, D.-B. Zhang, and T. Dumitrică, J. Phys. Chem. C **115**, 6392 (2011).
[34] D. G. Vercosa, E. B. Barros, A. G. Souza Filho, J. Mendes Filho, Ge. G. Samsonidze, R. Saito, and M. S. Dresselhaus, Phys. Rev. B **81**, 165430 (2010).
[35] D.-B. Zhang and T. Dumitrică, Appl. Phys. Lett. **93**, 031919 (2008).
[36] F. Ding, A. R. Harutyunyan, and B. I. Yakobson, Proc. Natl. Acad. Sci. USA **106**, 2506 (2009).
[37] L. Yang and J. Han, Phys. Rev. Lett. **85**, 154 (2000).
[38] E. Hernandez, C. Goze, P. Bernier, and A. Rubio, Phys. Rev. Lett. **80**, 4502 (1998).
[39] B. Akdim, R. Pachter, X. Duan, and W. W. Adams, Phys. Rev. B **67**, 245404 (2003).
[40] G. Y. Guo and J. C. Lin, Phys. Rev. B **71**, 165402 (2005).
[41] B. Baumeier, P. Kruger, and J. Pollmann, Phys. Rev. B **76**, 085407 (2007).
[42] T. Dumitrică and B. I. Yakobson, Phys. Rev. B **72**, 035418 (2005).
[43] N. Marom, J. Bernstein, J. Garel, A. Tkatchenko, E. Joselevich, L. Kronik, and O. Hod, Phys. Rev. Lett. **105**, 046801 (2010).
[44] V. N. Popov and L. Henrard, Phys. Rev. B **70**, 115407 (2004).
[45] G. Seifert (private communication).
[46] D.-B. Zhang, E. Akatyeva, and T. Dumitrică, Phys. Rev. Lett. **106**, 255503 (2011).